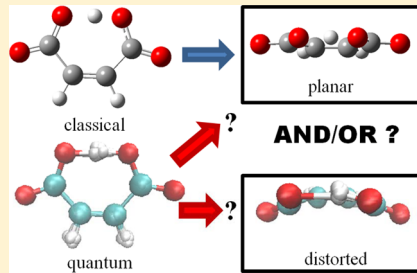


Ab Initio Path Integral Molecular Dynamics Study of the Nuclear Quantum Effect on Out-of-Plane Ring Deformation of Hydrogen Maleate Anion

Yukio Kawashima*,† and Masanori Tachikawa*

Quantum Chemistry Division, Graduate School of Science, Graduate School of Nanobioscience, Yokohama City University, Yokohama 236-0027, Japan

ABSTRACT: *Ab initio* path integral molecular dynamics (PIMD) simulation was performed to understand the nuclear quantum effect on the out-of-plane ring deformation of hydrogen maleate anion and investigate the existence of a stable structure with ring deformation, which was suggested in experimental observation (Filliaux et al., *Chem. Phys.* 1999, 120, 387–403). The isotope effect and the temperature effect are studied as well. We first investigated the nuclear quantum effect on the proton transfer. In static calculation and classical *ab initio* molecular dynamics simulations, the proton in the hydrogen bond is localized to either oxygen atom. On the other hand, the proton is located at the center of two oxygen atoms in quantum *ab initio* PIMD simulations. The nuclear quantum effect washes out the barrier of proton transfer. We next examined the nuclear quantum effect on the motion of hydrogen maleate anion. Principal component analysis revealed that the out-of-plane ring bending modes have dominant contribution to the entire molecular motion. In quantum *ab initio* PIMD simulations, structures with ring deformation were the global minimum for the deuterated isotope at 300 K. We analyzed the out-of-plane ring bending mode further and found that there are three minima along a ring distortion mode. We successfully found a stable structure with ring deformation of hydrogen maleate for the first time, to our knowledge, using theoretical calculation. The structures with ring deformation found in quantum simulation of the deuterated isotope allowed the proton transfer to occur more frequently than the planar structure. Static *ab initio* electronic structure calculation found that the structures with ring deformation have very small proton transfer barrier compared to the planar structure. We suggest that the “proton transfer driven” mechanism is the origin of stabilization for the structure with out-of-plane ring deformation.



1. INTRODUCTION

Hydrogen maleate anion H(OOC—CH=CH—COO)⁻ (HM, Figure 1) is one of the simplest symmetric intramolecular hydrogen bonded system with symmetric and short hydrogen bond. The hydrogen bond structure and dynamics of HM have been widely studied by both experimental^{1–17} and theoretical^{18–33} works. HM continues to receive certain attention because it is considered as a simple model for studying low-barrier hydrogen bonds (LBHB) in biomolecular systems.^{34–39} While the proton is localized on a heavy atom of either side in typical hydrogen bonds, shorter and stronger LBHB has the proton located at the center of the hydrogen bond. Thus, investigating the location of the proton or examining the symmetry of the hydrogen bond is essential to study systems with LBHB.

The main issue of the past studies on HM was the location of the proton in the hydrogen bond or the symmetry of the hydrogen bond. The symmetry of the hydrogen bond is well-known to depend on the environment. Neutron¹ and X-ray² diffraction, infrared (IR) and Raman spectra,^{3–6} inelastic neutron scattering,^{7–9} NMR,^{10,11} and calorimetry¹² studies have revealed that the hydrogen bond is very short with C_{2v} symmetry in crystal of potassium HM, where the proton is located at the center of the hydrogen bond. The hydrogen has

been found to be localized on one oxygen atom with C_s symmetry in crystal of sodium salt¹³ and in water.^{14,15} Studies in other environment have been performed as well.^{16,17} Another important topic of the past works on HM was the assignment of the OHO asymmetric vibration ($\gamma_a(\text{OHO})$). Many experimental efforts have been made to assign $\gamma_a(\text{OHO})$ employing IR and Raman spectra,^{3–6} and inelastic neutron scattering techniques;^{7–9} however, there is no clear successful observation of these bands so far. Filliaux et al. studied the dynamics of potassium HM crystal using inelastic neutron scattering. Three components found in the spectra at 500, 530, and 655 cm⁻¹ were assigned to $\gamma_a(\text{OHO})$. Filliaux et al. claimed that the three components arise from a very anharmonic potential function and can be regarded as an almost triply degenerate level. From the viewpoint that the crystal of potassium HM is symmetric, they suggested a proton potential function of $\gamma_a(\text{OHO})$ with three nonequivalent minima.⁹ They also found three components in the spectra at 155, 303, and 605 cm⁻¹ and assigned them to the out-of-plane ring (O₃—C₁—C₄—C₆—C₈—O₃—O₁₀) bending mode. Following the same line as in the case of $\gamma_a(\text{OHO})$, they proposed a similar potential

Received: September 10, 2013

Published: December 9, 2013

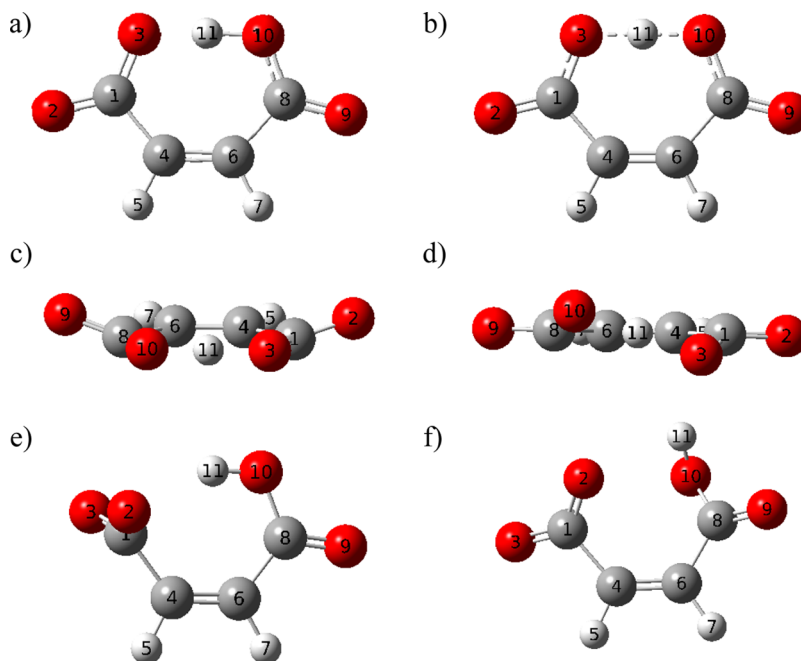


Figure 1. Structures of hydrogen maleate anion molecule with atom numbering for (a) equilibrium C_s structure, (b) transition state C_{2v} structure, (c) representative snapshot with plane symmetric distorted structure from quantum simulation, (d) representative snapshot with centrosymmetric distorted structure from quantum simulation, (e) transition state structure for dihedral angle rotation without hydrogen atom, and (f) transition state structure for dihedral angle rotation with hydrogen atom.

function of the out-of-plane ring bending mode with three nonequivalent minima shown in Figure 2. The potential

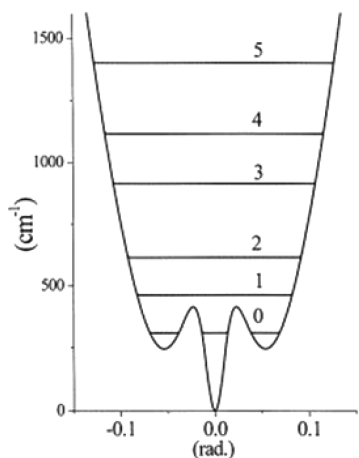


Figure 2. Potential function for the out-of-plane bending of the maleate ring proposed from inelastic neutron diffraction study. Reprinted with permission from ref 9. Copyright 1999, Elsevier B. V.

indicates the existence of a stable structure with out-of-plane ring deformation. However, the three nonequivalent minima have not been confirmed by other experimental work, and further investigation is necessary.

Many theoretical studies on HM were carried out to understand the symmetry of the hydrogen bond. Most of the works employed static *ab initio* electronic structure calculations, which results to a stable C_s symmetry hydrogen bond with proton localized on oxygen for isolated HM.^{18–30} Recent theoretical works found that C_{2v} symmetry hydrogen bond with the proton delocalized in the center of the hydrogen bond is more stable than C_s structure.^{32,33} These works are based on *ab*

initio path integral molecular dynamics (PIMD) simulation^{40–45} taking quantum effect of the electrons, thermal fluctuation, and nuclear quantum effect into account. These works show that consideration of the nuclear quantum effect on the hydrogen bond is essential to treat systems with short and symmetric hydrogen bonds. Dopieralski et al. employed PIMD simulation based on Car–Parrinello molecular dynamics to seek the environment effect on the hydrogen bond symmetry and proton dynamics of HM.³² Recently, we studied the isotope effect on the hydrogen bond structure of HM employing PIMD simulation based on Born–Oppenheimer molecular dynamics.³³ On the other hand, theoretical works on dynamics or fluctuation of the molecular system are limited to classical treatment of the proton.^{27–29} There are many efforts made to understand the proton transfer theoretically in general,^{46–48} but works studying quantum nuclear effect on fluctuation of the molecular system using PIMD simulation are scarce. Moreover, no theoretical work has explored the out-of-plane ring deformation of HM to confront or support the triple-minima potential surface proposed by Filliaux et al.,⁹ and a stable structure with out-of-plane ring deformation is not found so far to our knowledge.

In the present article, we report a theoretical study to investigate the nuclear quantum effect on molecular fluctuation, especially the out-of-plane ring bending motion of HM based on *ab initio* PIMD simulation, and seek the existence of stable structure with out-of-plane deformation suggested by Filliaux et al.⁹ We aim to analyze our simulation and explore the degrees of freedom which were not studied in previous works.^{32,33} Here, we consider quantum effect of electrons, thermal fluctuation of the system, and quantum fluctuation of the atomic nuclei in the simulations. Comparison with the conventional *ab initio* molecular dynamics (MD) simulation, in which quantum effect of electrons and thermal fluctuation of the system are taken into account, allows us to study the

Table 1. Hydrogen-Bond Lengths (Å) and Hydrogen-Bond Angle (deg) from Static Electronic Structure Calculations and Average Values from Simulation^a

	static calculation		classical simulation		quantum simulation			
	equilibrium	transition state	150 K	300 K	DM		HM	
			150 K	300 K	150 K	300 K	150 K	300 K
R_{OH^*}	1.324, 1.095	1.195	1.216(3)	1.227(3)	1.222(4)	1.229(3)	1.226(3)	1.231(3)
R_{OO}	2.418	2.388	2.427(1)	2.444(1)	2.428(2)	2.439(2)	2.430(2)	2.438(2)
$\angle \text{OH}^*\text{O}$	176.4	177.1	173.4(1)	170.8(1)	168.5(2)	167.7(2)	166.4(2)	166.1(2)

^aStatistical error of average values are given in parentheses.

nuclear quantum effect in details. We discuss isotope effect by analyzing the results of H-D substitution by performing PIMD simulation. We also perform simulations at 150 and 300 K to understand the temperature dependence of the nuclear quantum effect and understand the free energy surface of HM more clearly. Computational details are described in the section 2, the results in section 3, and concluding remarks in section 4.

2. COMPUTATIONAL DETAILS

Figure 1 shows various structures with the corresponding numbering of atoms for hydrogen maleate anion $\text{H(OOC—CH=CH—COO)}^-$ (HM). The global minimum structure and the transition state structure of HM, which shares a hydrogen-bonded proton H_{11} (later labeled as H^*) in the center of two oxygen atoms, are illustrated in Figure 1a and b. To seek the isotope effect of the proton transfer in the intramolecular hydrogen bond, we also calculated $\text{D(OOC—CD=CD—COO)}^-$ (DM) with hydrogen-bonded deuteron D_{11} (later labeled as D^*).

All electronic structure calculations were performed employing ωB97XD ⁴⁹ with 6-31G** basis set with additional diffused basis functions for oxygen atoms. In our previous study, we investigated the proton transfer barrier height of HM using static *ab initio* calculation. The proton transfer barrier height using CCSD(T)/aug-cc-pVDZ optimized structures was 0.21 kcal/mol. MP2 and B3LYP methods underestimated this value, while ωB97XD method estimated values in between MP2 and CCSD(T). The barrier height calculated by ωB97XD with 6-31G** basis set with additional diffused basis functions for oxygen atom was 0.12 kcal/mol, which was in reasonable agreement with CCSD(T) calculated value. We thus used the above-mentioned level for our simulations.

The HM structure does not retain the planar structures, as shown in Figure 1a and b, as it is quite flexible. The representative snapshots of ring-distorted structures from our simulation are shown in Figure 1c and d. We note here that structures with broken hydrogen bonds due to out-of-plane ring distortion, depicted in Figure 1e and f, were not found in our simulations. The barrier heights of the rotation calculated by intrinsic reaction coordinates to obtain these structures are 14.0 and 24.4 kcal/mol, respectively. Structures were flexible, but the intramolecular hydrogen bond was retained in our simulation at 150 and 300 K due to the high rotation barriers.

The calculation methods mostly follow the procedure in our previous work.³³ On-the-fly *ab initio* PIMD and MD simulations were carried out at 300 and 150 K with Nosé–Hoover chain thermostats⁵⁰ to achieve a canonical ensemble. The numbers of the classical beads to describe the atomic nucleus are 32, 16, and 1 beads, for PIMD at 150 K, PIMD at 300 K, and *ab initio* MD simulations, respectively. We later

denote the simulations assumed to be quantum (PIMD) and classical (MD) nuclei as “quantum” and “classical” simulations. For quantum simulations, we used normal mode transformation to isolate the time scales associated with the different mode and the Nosé–Hoover chain thermostats were attached to each degree of freedom (3NP sets) to overcome the lack of ergodicity as recommended by Tuckerman et al.⁵¹

For quantum simulation, we performed two simulations: one with hydrogen atoms, and one substituting all hydrogen atoms with deuterium atoms. The quantum (classical) simulations were carried out for 90 000 (760 000) steps after thermal equilibration run of 10 000 (40 000) steps with a time step of 0.1 (0.1) fs. As for DM, the time step of 0.15 fs was used. *Gaussian09*⁵² was used for electronic structure calculation.

We examined the hydrogen-bond fluctuation with geometric parameters: the difference between two O–H* bond lengths ($\delta_{\text{OH}^*} = R_{\text{O}_3\text{H}^*} - R_{\text{O}_{10}\text{H}^*}$), the distance between two oxygen atoms of O_3 and O_{10} (R_{OO}), and the bond angle of $\text{O}_3\text{—H}^*\text{—O}_{10}$ ($\angle \text{OH}^*\text{O}$). The dihedral angle $\text{O}_3\text{—C}_1\text{—C}_8\text{—O}_{10}$ ($\angle \text{OCCO}$), influenced by the hydrogen bond fluctuation, is also studied. For DM, the difference between two OD* bond lengths is later denoted as δ_{OH^*} and bond angle $\text{O}_3\text{—D}^*\text{—O}_{10}$ is denoted as $\angle \text{OH}^*\text{O}$. We note here that $\delta_{\text{OH}^*} = 0$ is interpreted as that the H^* atom is located at the midsection of the two hydrogen atoms with the symmetry of C_{2v} , while a large absolute δ_{OH^*} value is interpreted as that H^* is localized on either atom with C_s symmetry.

We performed principal component analysis (PCA)^{53–56} to understand the molecular motion of HM and DM. We first obtained the averaged structure for all simulations. Next, we constructed a variance–covariance matrix and diagonalized it. Here, we removed all six degrees of freedom of the center of mass: three for translation and three for rotation. The obtained eigenvectors correspond to the principal component (PC) axes. The PC with the largest eigenvalue, or in other words, with the largest contribution to the entire molecular motion, is the first PC. Normal mode analysis using optimized structure from static *ab initio* calculation was carried out for comparison.

We constructed two-dimensional free-energy landscapes with various collective variables from quantum and classical simulations. The free energies of the landscapes are defined as

$$F = -k_B T (\ln(P(x, y)) - \ln(P(x_{\max}, y_{\max}))) \quad (1)$$

Variables k_B is the Boltzmann constant, T is the temperature, and $P(x, y)$ is the probability distribution of configurations with structural parameters x and y . $P(x_{\max}, y_{\max})$ is the region with maximum probability with structural parameters x_{\max} and y_{\max} where the free energy is set to 0.0.

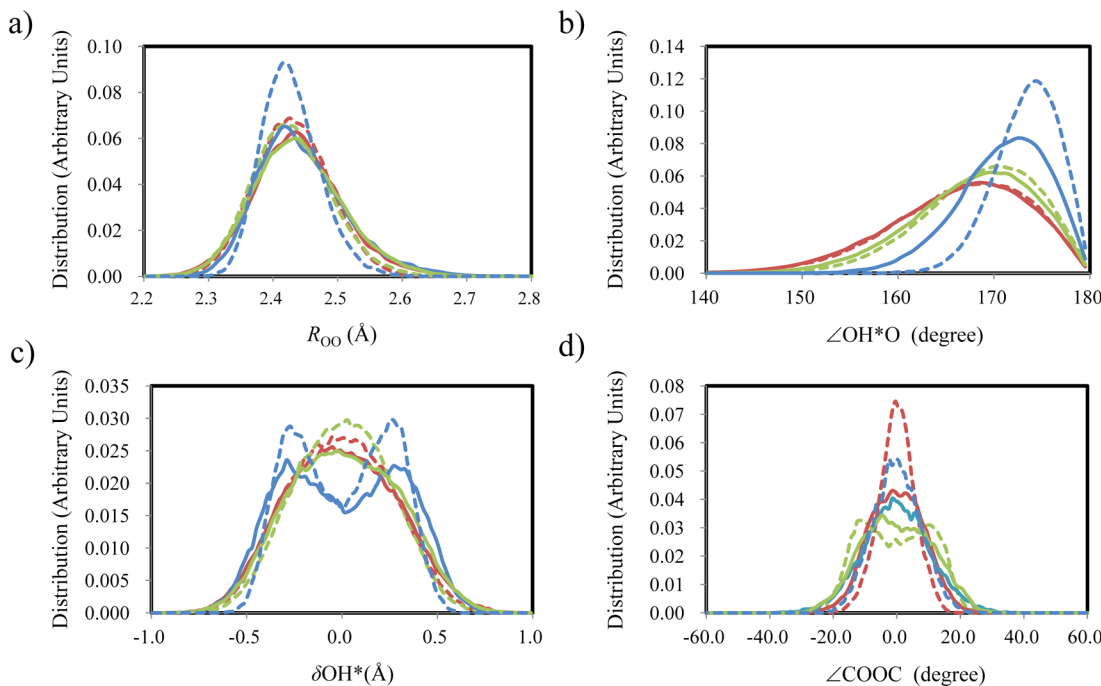


Figure 3. Distributions of (a) R_{OO} , (b) $\angle \text{OH}^*\text{O}$, (c) δ_{OH^*} , and (d) $\angle \text{COOC}$ by classical simulation (blue line), quantum simulations for DM (green line), and quantum simulation for HM (red line). The solid and dashed lines represent simulations at 300 and 150 K, respectively.

3. RESULTS AND DISCUSSION

3.1. Hydrogen Bond Structure in Quantum and Classical Simulations. Hydrogen bond lengths R_{OH^*} and R_{OO} with angle $\angle \text{OH}^*\text{O}$, obtained from static electronic structure calculations, and average bond lengths and angle calculated from quantum and classical simulations are described in Table 1. Their statistical errors described in parentheses were calculated using the blocking method.⁵⁷ Distributions of the parameters for the hydrogen bond structure are illustrated in Figure 3, where distributions of R_{OO} and $\angle \text{OH}^*\text{O}$ obtained from the simulations are shown in parts a and b of Figure 3, respectively.

Two R_{OH^*} values are listed in Table 1 for the equilibrium structure optimized by static calculation, because H^* is localized on one of the oxygen atoms ($\text{OH}^* \cdots \text{O}$) in the global minimum structure with C_s symmetry, as shown in Figure 1a. On the other hand, the transition state structure has only one value since the proton is located at the center of two oxygen atoms with C_{2v} structure as described in Figure 1b. The relation of R_{OH^*} values are found to be

$$\begin{aligned} R_{\text{OH}^*}^{(\text{EQ})} &< R_{\text{OH}^*}^{(\text{TS})} \ll \langle R_{\text{OH}^*} \rangle^{\text{cl } 150} < \langle R_{\text{OH}^*} \rangle^{\text{D } 150} < \langle R_{\text{OH}^*} \rangle^{\text{H } 150} \\ &\leq \langle R_{\text{OH}^*} \rangle^{\text{cl } 300} < \langle R_{\text{OH}^*} \rangle^{\text{D } 300} < \langle R_{\text{OH}^*} \rangle^{\text{H } 300} \end{aligned} \quad (2)$$

where superscript “cl” represents classical simulation and “H” and “D” the quantum simulations of HM and DM, respectively. The numbers “150” and “300” following these superscripts represent the temperature of the simulations 150 and 300 K, respectively. As found in our previous work, temperature effect elongates the OH^* bond.³³ This is also confirmed in this work by comparing bond length at 150 and 300 K. Bond length at higher temperature 300 K has longer bond length than at 150 K. The difference between quantum simulation and classical simulation is larger at 150 K than at 300 K. This shows that the nuclear quantum effect is larger at lower temperature. The isotope effect, the difference between HM and DM, is also

larger at 150 K as well. This also reflects the large nuclear quantum effect at low temperature.

Table 1 shows that the relation of average O–O bond length among the simulations is

$$\begin{aligned} R_{\text{OO}}^{(\text{TS})} &< R_{\text{OO}}^{(\text{EQ})} \ll \langle R_{\text{OO}} \rangle^{\text{cl } 150} \approx \langle R_{\text{OO}} \rangle^{\text{D } 150} \\ &< \langle R_{\text{OO}} \rangle^{\text{H } 150} \ll \langle R_{\text{OO}} \rangle^{\text{H } 300} \approx \langle R_{\text{OO}} \rangle^{\text{D } 300} < \langle R_{\text{OO}} \rangle^{\text{cl } 300} \end{aligned} \quad (3)$$

where the tendency is different from the inequality in eq 2. The average R_{OO} of classical simulation is longer than the optimized bond length of both equilibrium and transition state structures in static calculation due to thermal effect, which is also confirmed by comparing simulation results of 150 and 300 K. The bond lengths of simulations at 300 K are longer than that at 150 K. The difference among the simulation is very small at 150 K; however, the tendency found at 150 K is different from 300 K. The bond length found in classical simulation is the longest and the bond is slightly longer in DM than HM at 300 K, while the bond in classical simulation is the shortest and DM is shorter than HM at 150 K. The distribution of R_{OO} shown in Figure 3a finds very small quantum effect and isotope effect. The difference among the distributions is rather small. The classical simulation at 150 K shows a narrow distribution compared to other distributions, which shows that the temperature effect on the bond length distribution is large for classical simulations. The difference in the relation of the bond lengths among simulations at 150 and 300 K reflects the variance in the temperature effect on the nuclear quantum effect.

The relation of the hydrogen bond angle $\angle \text{OH}^*\text{O}$ among the simulations is as follows:

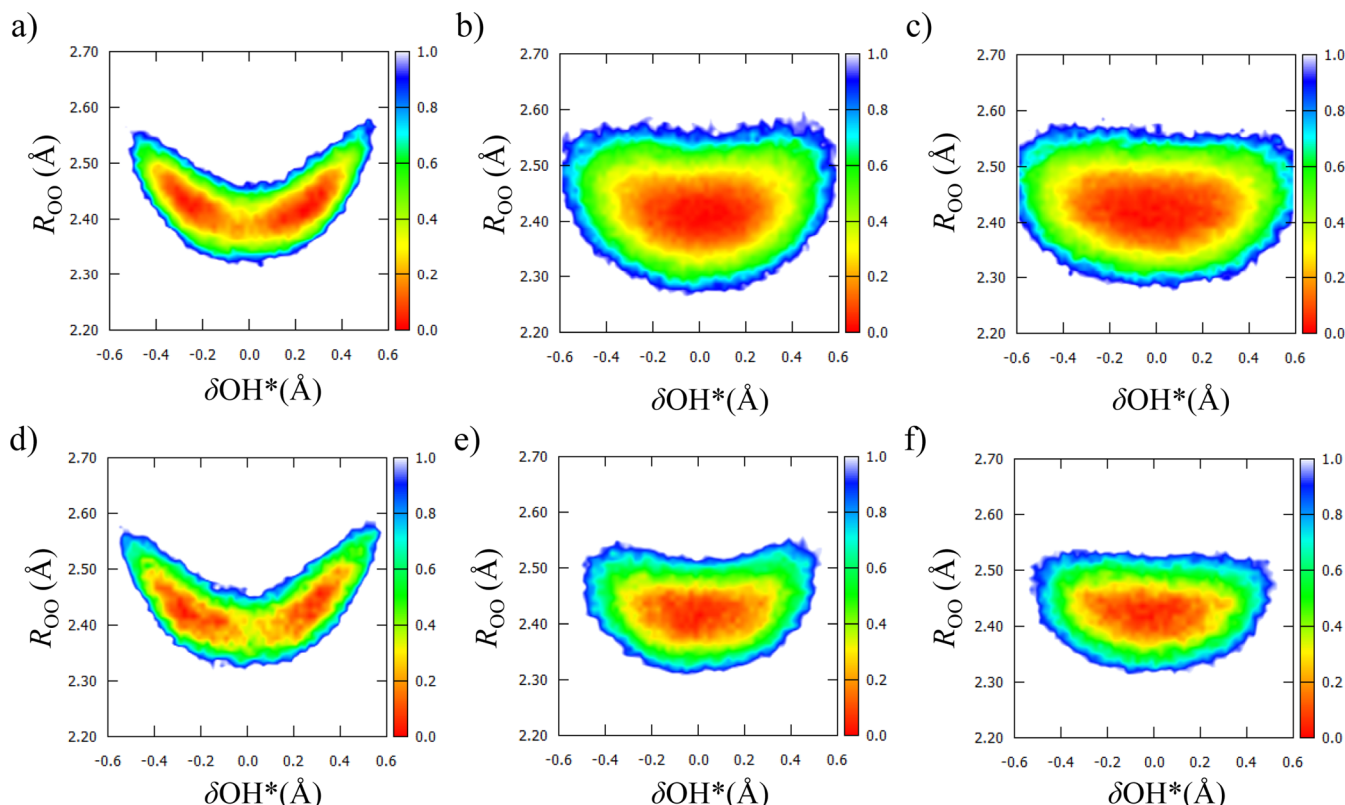


Figure 4. Two-dimensional free-energy landscape of δ_{OH^*} and R_{OO} for (a) classical simulation at 150 K, (b) quantum simulation for DM at 150 K, (c) quantum simulation for HM at 150 K, (d) classical simulation at 300 K, (e) quantum simulation for DM at 300 K, (f) quantum simulation for HM at 300 K. The unit of free energy (potential of mean force) is kcal/mol.

$$\begin{aligned} \langle \angle \text{OH}^* \text{O} \rangle^{\text{H}300} &\approx \langle \angle \text{OH}^* \text{O} \rangle^{\text{H}150} < \langle \angle \text{OH}^* \text{O} \rangle^{\text{D}300} \\ &< \langle \angle \text{OH}^* \text{O} \rangle^{\text{D}150} < \langle \angle \text{OH}^* \text{O} \rangle^{\text{cl } 300} < \langle \angle \text{OH}^* \text{O} \rangle^{\text{cl } 150} \\ &< \angle \text{OH}^* \text{O}^{\text{(EQ)}} < \angle \text{OH}^* \text{O}^{\text{(TS)}} \end{aligned} \quad (4)$$

The average values found in the simulations are smaller than those of optimized structures in static calculation due to thermal fluctuation, as listed in Table 1. This is also confirmed by comparing larger angle found in 150 K with smaller angle found in 300 K. The average value obtained from quantum simulation is smaller than that of classical simulation. The distributions of $\angle \text{OH}^* \text{O}$ are displayed in Figure 3b. The distribution of quantum simulation is wider than that from classical simulation, and the peak is shifted to a smaller value. Anharmonic quantum fluctuation bends the hydrogen bond, which results to the shift to the smaller region in quantum simulation compared to the classically obtained angle distribution. Large isotope effect is found in the distribution of hydrogen-bond angle. The distribution of average bond angle in HM is wider than DM, which indicates that the anharmonic quantum fluctuation is smaller for DM than HM. The difference among simulations is larger at 150 K than 300 K. The reduction of the thermal effect makes nuclear quantum effect on $\angle \text{OH}^* \text{O}$ more apparent.

3.2. Quantum Effect on the Proton Transfer. We analyze the proton transfer coordinate δ_{OH^*} for understanding the location of H^* in the hydrogen bond or, in other words, the hydrogen-bond symmetry of the intramolecular hydrogen bond. Distribution of δ_{OH^*} found in quantum and classical simulations are depicted in Figure 3c.

The classical simulation shows two peaks with large absolute δ_{OH^*} values. The dominant hydrogen-bond structure found in classical simulation for both 150 and 300 K has C_s symmetry, or H^* is localized on one oxygen atom. The localization of the proton on oxygen atom at both ends of the hydrogen bond is stronger at 150 K than at 300 K. The distributions of quantum simulations show one dominant peak at $\delta_{\text{OH}^*} = 0$, which shows that H^* is located at the center of two oxygen atoms or the hydrogen bond has C_{2v} symmetry. This clearly shows that nuclear quantum effect leads to barrier-less proton transfer. No significant isotope effect is found in δ_{OH^*} distribution.

We constructed two-dimensional free-energy landscape from two-dimensional distribution of δ_{OH^*} and R_{OO} , illustrated in Figure 4, for further analysis on the proton transfer. As shown in Figure 4a and d, the free-energy surfaces obtained from classical simulations have two minima, while Figures 4b, c, e, and f constructed from quantum simulations have one minimum. The nuclear quantum effect washes out the proton transfer barrier completely allowing barrier-less proton transfer. Smaller thermal fluctuation at 150 K results to a more dense distribution around the proton transfer coordinate. The isotope effect on these free-energy surfaces of quantum simulation is rather small.

In our previous work, we roughly estimated the effective barrier height for proton transfer by fixing R_{OO} (and R_{OH^*} at the transition state) at the averaged values of quantum and classical simulations. We estimated the barrier height for quantum simulation of HM, DM, and the classical simulation at 300 K, as 0.46, 0.47, and 0.53 kcal/mol, respectively. The barrier is low and it is washed out completely for quantum simulations. The barrier height obtained from static calculation using the same

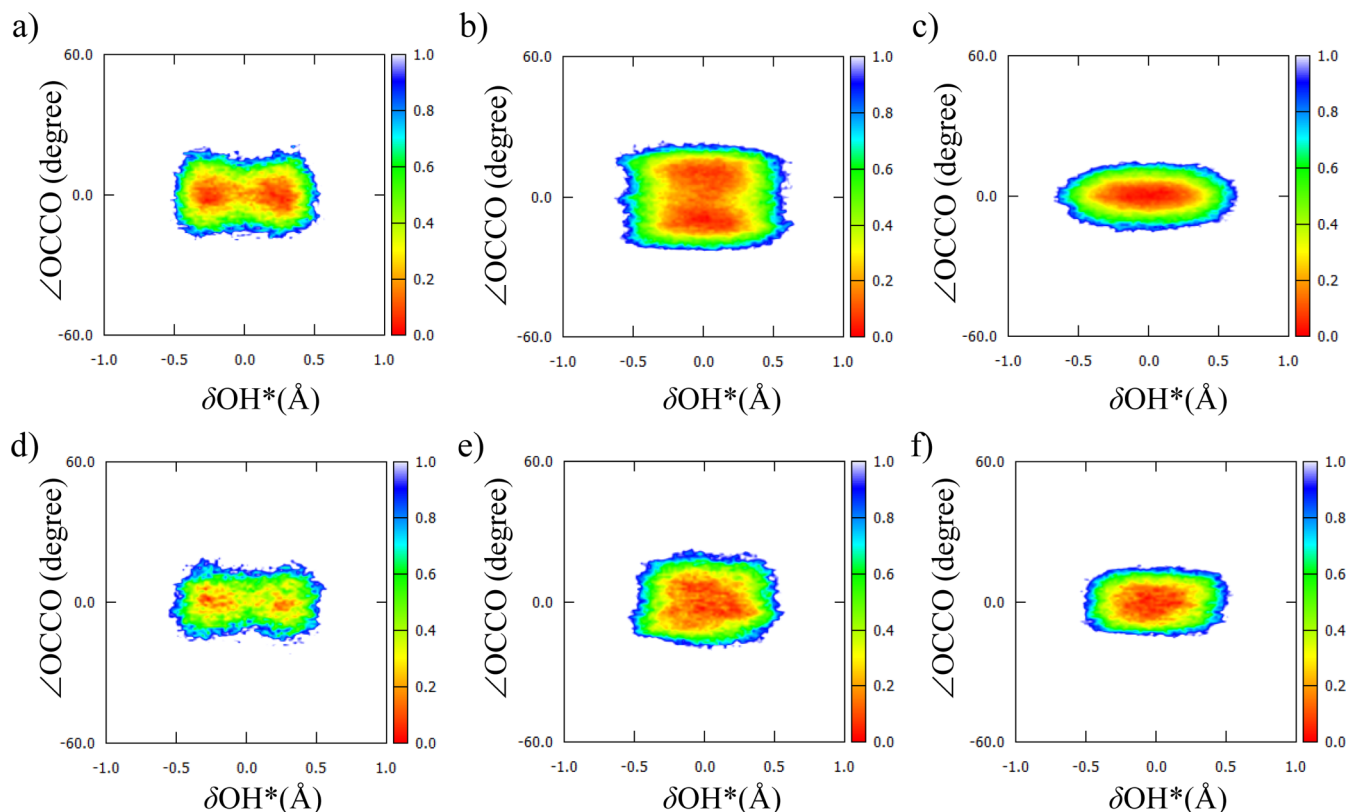


Figure 5. Two-dimensional free-energy landscape of δ_{OH^*} and $\angle \text{OCCO}$ for (a) classical simulation at 150 K, (b) quantum simulation for DM at 150 K, (c) quantum simulation for HM at 150 K, (d) classical simulation at 300 K, (e) quantum simulation for DM at 300 K, (f) quantum simulation for HM at 300 K. The unit of free energy (potential of mean force) is kcal/mol.

Table 2. Harmonic Vibrational Frequency (cm^{-1}) of Lowest Ring Distortion Modes and the Contribution of These Modes (%) to the Entire Molecular Motion Obtained from Principle Component Analysis

	normal mode analysis		principle component analysis					
	harmonic vibrational frequency (cm^{-1})		contribution of each vibrational mode (%)					
	D	H	Cl		D		H	
			150 K	300 K	150 K	300 K	150 K	300 K
Mode 1	58.4	60.3	63	63	21	62	44	17
Mode 2	106.5	106.7	19	20	44	18	11	25
Mode 3	271.1	286.7	3 (4)	3 (3)	3 (4)	2 (5)	5 (3)	13 (3)

The ordinal number of PC corresponding to Mode 3 in principle component analysis is in parentheses.

level of theory as in the simulations was 0.12 kcal/mol. Surprisingly, the proton transfer barrier height is larger in classical simulation and could not overcome the low barrier height of 0.12 kcal/mol. This is originated from the elongation of R_{OO} due to the thermal fluctuation at 300 K. The heightening of the barrier height was also reported by Tuckerman and Marx in their work on the PIMD simulation of malonaldehyde.⁵⁸ The proton transfer barrier was not washed out completely in their quantum simulation because of the large barrier height of the intramolecular hydrogen bond proton transfer of about 3.5 kcal/mol. Simulations at 150 K has shorter R_{OO} compared to 300 K, therefore, the barrier height will become smaller.

3.3. Dihedral Angle of the Hydrogen Bond. We next focused on an additional geometric parameter of the hydrogen bond: dihedral angle $\text{O}_3-\text{C}_1-\text{C}_8-\text{O}_{10}$ ($\angle \text{OCCO}$). The dihedral angle is related to the hydrogen bond fluctuation and is a good

index to seek the out-of-plane ring deformation. The distributions of the dihedral angle are illustrated in Figure 3d. These distributions show large thermal effect: distributions for simulations at 150 K are localized compared to those at 300 K. While distributions of quantum simulation for HM have a sharp peak at the center, distributions of classical simulations are slightly more broadened. Large isotope effect was found in the distribution of dihedral angle. Distributions of DM show broad distribution compared to other simulations, which indicates that the ring deformation is large.

We constructed two-dimensional free-energy landscape from two-dimensional distribution of δ_{OH^*} and $\angle \text{OCCO}$, described in Figure 5, to investigate the relation between proton transfer and fluctuation of the dihedral angle. Distributions of classical simulations, shown in Figure 5a and d, have two peaks as in Figure 4a and d. These distributions show that large fluctuation in the dihedral angle is found when the proton is localized on

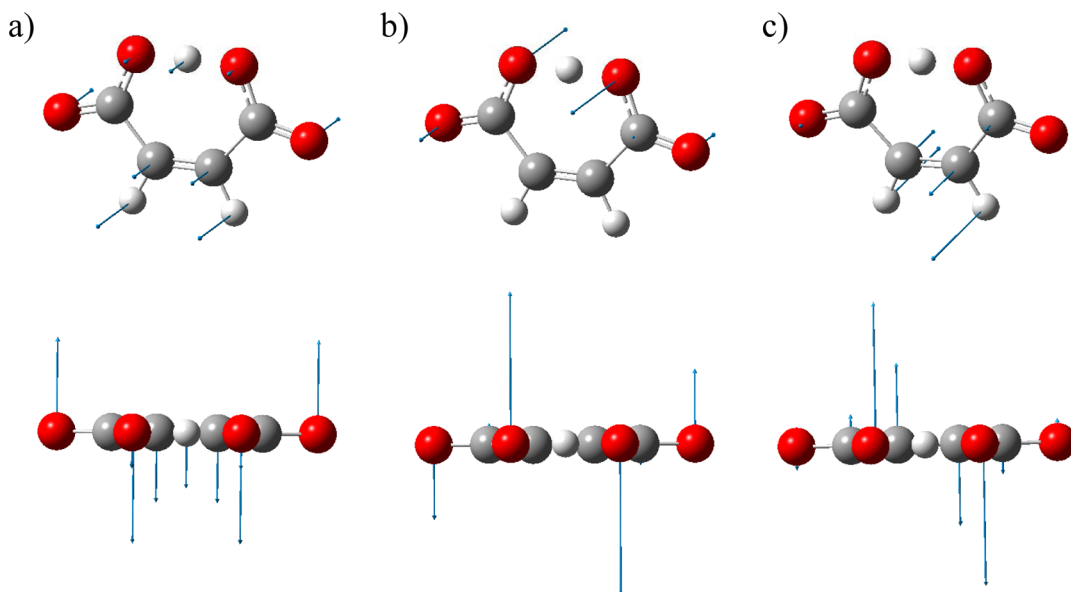


Figure 6. Displacement vectors of vibration for the three lowest frequencies in normal-mode analysis: (a) Mode 1, (b) Mode 2, and (c) Mode 3.

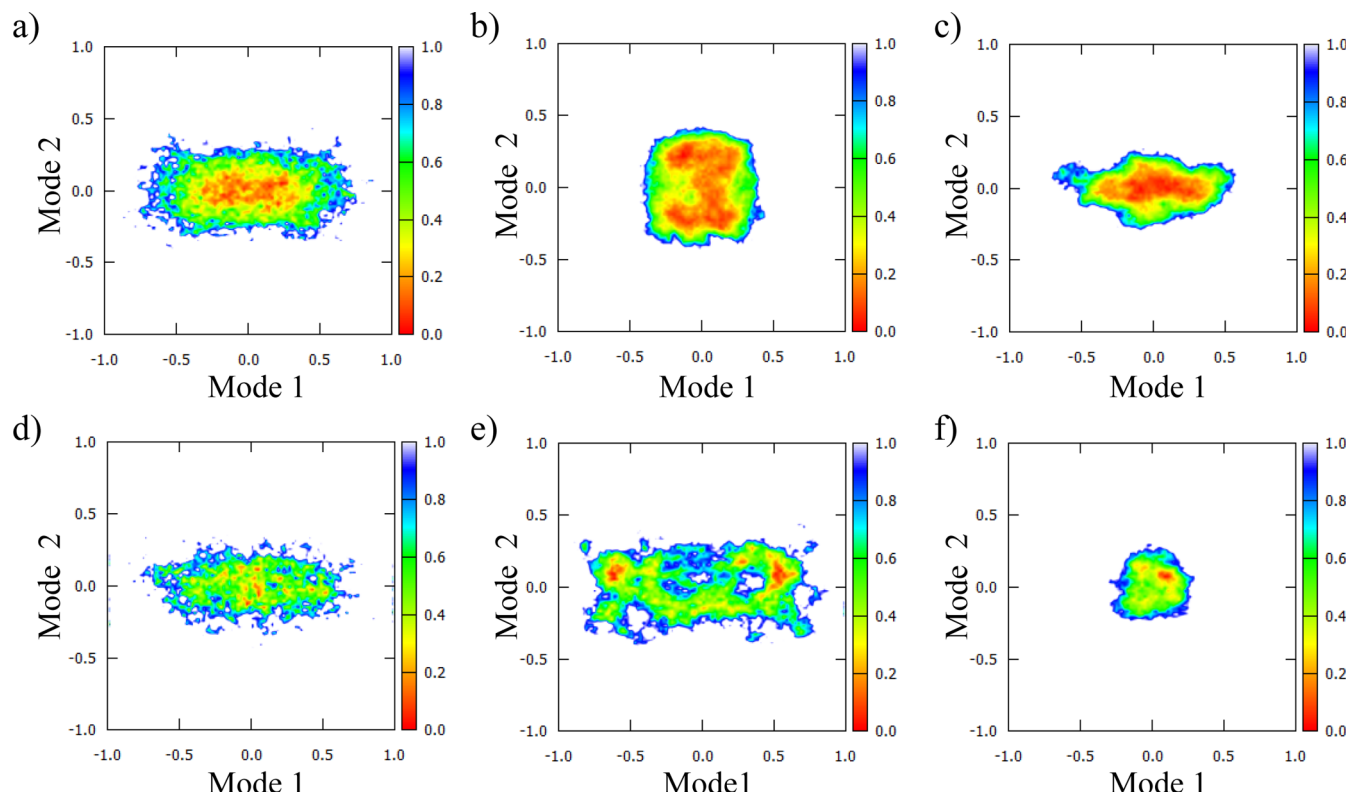


Figure 7. Two-dimensional free-energy landscape of the first two PCs corresponding to Mode 1 and Mode 2 in normal-mode analysis for (a) classical simulation at 150 K, (b) quantum simulation for DM at 150 K, (c) quantum simulation for HM at 150 K, (d) classical simulation at 300 K, (e) quantum simulation for DM at 300 K, (f) quantum simulation for HM at 300 K. The unit of free energies (potential of mean force) is kcal/mol.

the heavy atom at both ends of the hydrogen bond. The distributions of quantum simulation for HM, shown in Figure 5c and f, have a single peak at the center, where the ring is planar and the proton is located at the center of the hydrogen bond. Thermal effect results to a wider distribution in the dihedral angle. Meanwhile, quantum simulation for DM has a broad distribution in the dihedral angle as described in Figure 5b and e. At 150 K, distribution in the dihedral angle is very wide and distribution around $\angle\text{OCCO} = 0^\circ$ is sparse compared

to HM. Moreover, the distribution in this region has narrow distribution along the proton transfer coordinate, while proton transfer seems to be more frequent at large absolute $\angle\text{OCCO}$ values. This indicates that DM at 150 K favors structures with ring deformation and proton transfer occurs more frequently in these structures. Distribution of DM at 300 K lies in between DM at 150 K and HM. The distribution around $\angle\text{OCCO} = 0^\circ$ is not as sparse compared to DM at 150 K but is sparse compared to HM. Overall, in quantum simulation of DM,

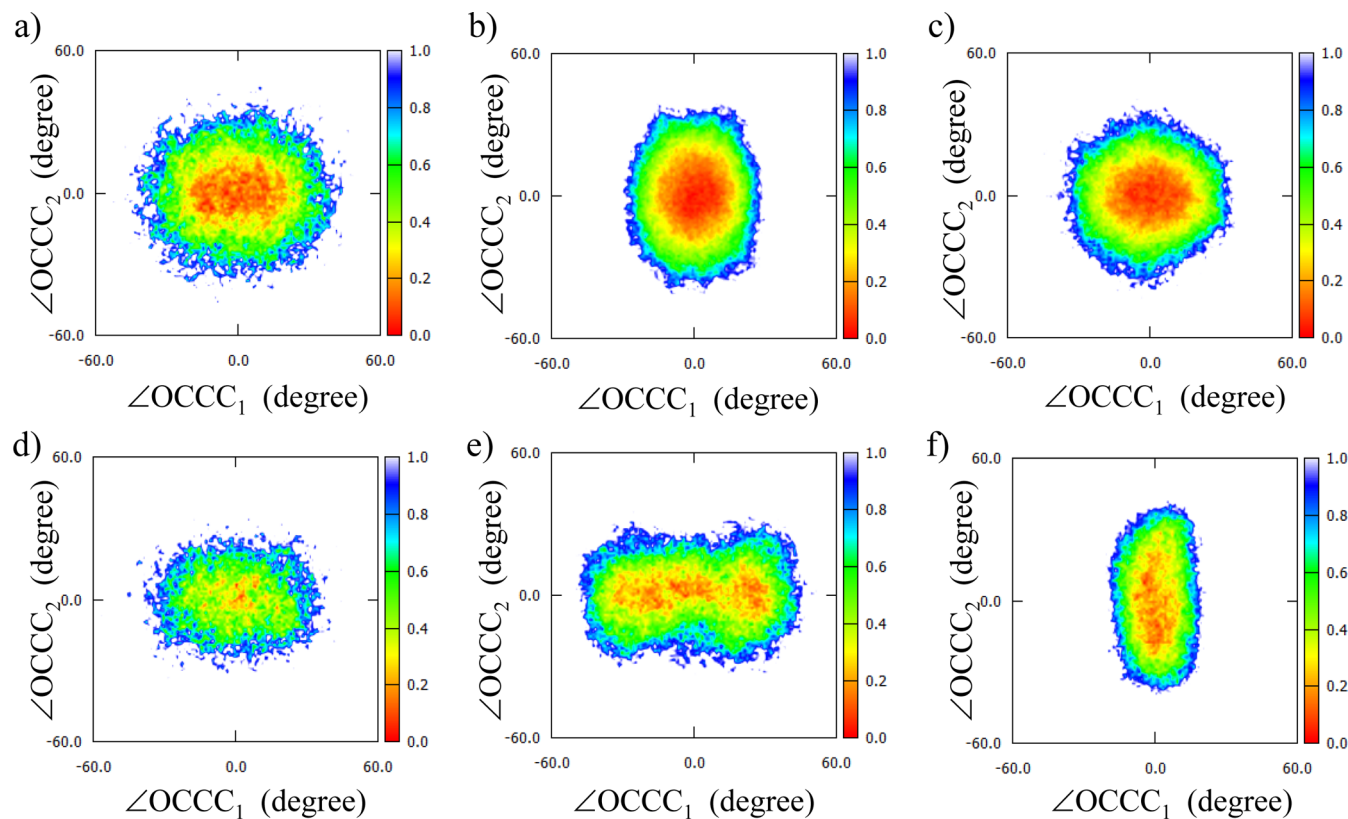


Figure 8. Two-dimensional free-energy landscape of $\angle \text{OCCC}_1$ and $\angle \text{OCCC}_2$ for (a) classical simulation at 150 K, (b) quantum simulation for DM at 150 K, (c) quantum simulation for HM at 150 K, (d) classical simulation at 300 K, (e) quantum simulation for DM at 300 K, (f) quantum simulation for HM at 300 K. The unit of free energy (potential of mean force) is kcal/mol.

proton transfer occurs more frequently at structures with out-of-plane ring deformation.

3.4. Principal Component Analysis. We have carried out normal-mode analysis to understand the low-frequency molecular vibration of HM. The harmonic vibrational frequencies of the three lowest modes are listed in Table 2, and the displacement vectors of these modes are shown in Figure 6. The three modes are all described as out-of-plane ring bending motions. The frequencies for these modes are 60.3, 106.7, and 286.7 cm^{-1} for HM, and 58.4, 106.5, and 271.1 cm^{-1} for DM. We later denote these modes as Mode 1, Mode 2, and Mode 3, respectively. Isotope effect is small for the first two modes.

We performed PCA to understand the dominating molecular motions in the simulations. We note that there are other studies employing PCA to study the vibration of molecules from molecular dynamics simulation. Pirc et al. employed PCA to understand the correlation between OH vibration and various geometric parameters,⁵⁹ while we have employed PCA to understand the nuclear quantum effect on the molecular fluctuations by obtaining new degree of freedom for describing the fluctuation of the molecule. We found that the PCs with large contribution to the molecular motion are the out-of-plane ring bending modes as found in normal-mode analysis. The ratios of the contribution to the entire molecular motion, namely, the ratios of the eigenvalues of the PCs corresponding to Modes 1–3 are listed in Table 2. The first two PCs with largest contribution to the molecular motion matched completely with the two lowest modes in normal-mode analysis: Mode 1 and Mode 2. The ordinal number of the PC corresponding to Mode 3 obtained from PCA in each

simulation, are listed in parentheses shown in Table 2. We note that the difference in contribution besides the first two PCs is very small. The contribution in the classical simulations has the same tendency with normal-mode analysis. The PCs with large components corresponded to the softest modes. Mode 1 has the largest contribution to the entire molecular motion, and Mode 2 has the second largest. Thermal effect was very small in classical simulations. We found large thermal effect in the PCA results for quantum simulations. The contribution of Mode 1 in quantum simulation for HM at 150 K was the largest as found in classical simulations, but the contribution of Mode 2 becomes the largest at 300 K. The origin of the increase of contribution from Mode 2 can be interpreted as the increase of the contribution from vibrational excitation due to thermal effect. On the other hand, PCA results for quantum simulation of DM show a peculiar behavior. The tendency found in the contribution from the modes found in quantum simulation of DM is the opposite from the quantum simulation of HM. Large isotope effect is found in molecular motion of quantum simulations.

Further examination was carried out by constructing two-dimensional free energy landscape projecting each configuration on to the first two principal axes, corresponding to Mode 1 and Mode 2, which is given as the potential of mean force with principal component axes as reaction coordinates. The free energy landscapes are depicted in Figure 7. For classical simulations and quantum simulations of HM, the free energy landscapes shown in Figure 7a, c, d, and f are all described as a single distribution with the minimum at the center, which corresponds to the average structure. This indicates that the distribution is centered at the planar

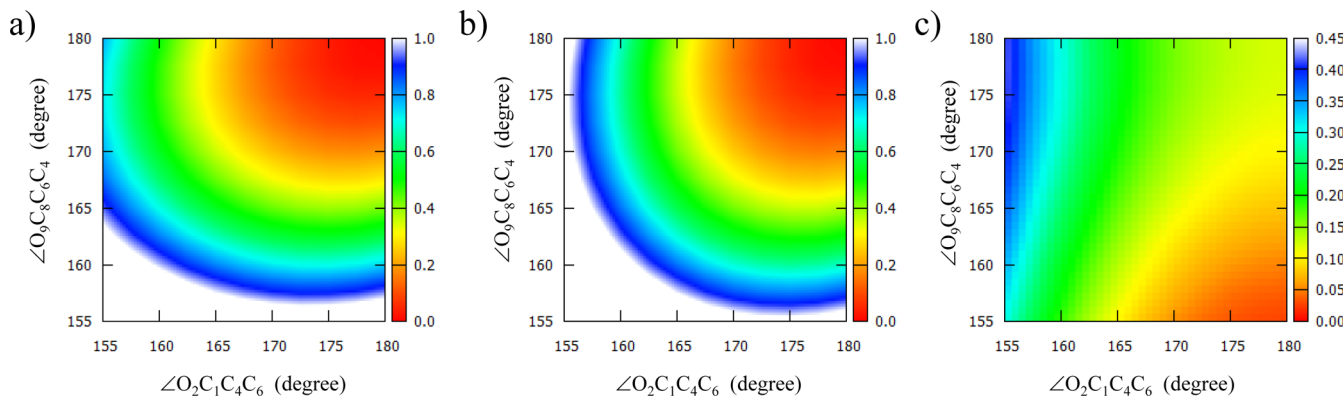


Figure 9. Two-dimensional potential energy surface of $\angle O_2C_1C_4C_6$ and $\angle O_9C_8C_6C_4$ for (a) E_{C_s} , (b) E_{C_v} , and (c) E_{PT} . The unit of potential energy is kcal/mol.

structure. The minimum of the free energy landscape of DM at 150 K is located at the center; however, there are two minima located far from the center along the PC1 axis at 300 K. This indicates that the structures with out-of-plane ring deformation are more favored than planar structures for DM at 300 K.

3.5. Out-of-Plane Ring Deformation of Hydrogen Maleate Anion.

We next simplified the free-energy landscape from the two PCs to focus on the out-of-plane ring deformation. We constructed a two-dimensional free-energy landscape from two geometric parameters: $\angle O_2C_1C_4C_6 + \angle O_9C_8C_6C_4$ and $\angle O_3C_1C_4C_6 - \angle O_{10}C_8C_6C_4$. The former parameter mimics Mode 1 and the latter mimics Mode 2. We later denote these parameters as $\angle OCCC_1$ and $\angle OCCC_2$, respectively. Large absolute $\angle OCCC_1$ values correspond to structures shown in Figure 1c, and large absolute $\angle OCCC_2$ values correspond to structures shown in Figure 1d. The free energy landscapes are illustrated in Figure 8. Simulations at 150 K have dense distribution at the center indicating that the molecular structure is fluctuating near the planar structure, while the structure is more widely distributed with less area of small free energy region at 300 K. For classical simulations, the distribution is larger in the $\angle OCCC_1$ axis, reflecting the dominant Mode 1 contribution to the entire molecular motion. For quantum simulation of HM, the shape of the distribution differs among simulations at 150 and 300 K. The distribution is larger in the $\angle OCCC_1$ axis for simulation at 150 K, while it is larger in the $\angle OCCC_2$ axis at 300 K. This reflects the PCA results with dominant contribution of Mode 1 at 150 K, and that of Mode 2 at 300 K. For quantum simulation of DM, the difference between the distribution at 150 and 300 K is significant. At 150 K, the distribution is described as a single peak at the center with wider distribution in the $\angle OCCC_2$ axis corresponding to the dominant contribution from Mode 2 as found in PCA. At 300 K, we found three minima in the $\angle OCCC_1$ axis, which have wider distribution reflecting the dominant Mode 1 contribution. This shows that structures with ring deformation are stable as the planar structure at 300 K for DM.

In the work by Filliaux et al.,⁹ the potential of the out-of-plane ring deformation was described by a triple-minima surface as shown in Figure 2. Their work indicated the existence of a minimum with structure of out-of-plane ring deformation as well as the planar structure. Coincidentally, we found three minima in the free energy landscape shown in Figure 8. This minimum was not found in static *ab initio* electronic structure calculation. It is difficult to find direct correspondence with the

work by Filliaux et al.,⁹ however, we succeeded in finding a stable structure with out-of-plane ring deformation in addition to the planar symmetric structure.

The interpretation of the PCA result of DM can be made by using the surface proposed by Filliaux et al.⁹ shown in Figure 2. At 150 K, the dominant distribution is localized in one minimum at the center in Figure 2, and some contribution of vibrational excitation arises. At 300 K, the distribution localizes because the trajectory is trapped in other minima at the right and left side in Figure 2, and the contribution from vibrational excitation does not arise. We suggest this as the origin of the peculiar behavior found in quantum simulation of DM.

3.6. Origin of the Stable Out-of-Plane Ring-Distorted Structure.

We constructed a two-dimensional potential energy surface from static *ab initio* electronic structure calculation to understand the origin of the stable structure with out-of-plane ring deformation found in simulation of DM at 300 K. We used two dihedral angles to describe the ring deformation: $\angle O_2C_1C_4C_6$ and $\angle O_9C_8C_6C_4$. The potential energy surfaces are constructed by freezing the dihedral angles and optimizing the remaining degrees of freedom. The constructed potential energy surfaces are described in Figure 9.

Figure 9a shows the potential energy surface of structure with a proton localized on O_{10} . The structure with both dihedral angles at 180° is the C_s structure shown in Figure 1a. We later on denote the potential energy of this surface as E_{C_s} . The potential energy surface shows that the rotation of $\angle O_2C_1C_4C_6$ is more stable than $\angle O_9C_8C_6C_4$. This corresponds to the difference in the rotational barrier height of the two dihedral angles. The two rotations are described in Figure 1e and f, respectively. The rotation of the dihedral angle $\angle O_2C_1C_4C_6$, without the covalently bonded hydrogen atom, have a barrier height of 14.0 kcal/mol, while the rotation of the dihedral angle $\angle O_9C_8C_6C_4$, with the covalently bonded hydrogen atom, has a larger barrier height of 24.4 kcal/mol. Hence, the proton transfer becomes asymmetric. On the other hand, the potential energy surface shown in Figure 9b was constructed forcing the proton in the center of two oxygen atoms. The structure with both dihedral angles at 180° is the C_{2v} structure, illustrated in Figure 1b. We later on denote the potential energy of this surface as E_{C_v} . The potential energy surface is symmetric.

The proton transfer barrier E_{PT} for out-of-plane distorted ring structures in each point of the potential energy surface is obtained as follows,

$$E_{\text{PT}} = E_{C_{2v}} - E_{C_s} \quad (5)$$

We show the potential energy surface of E_{PT} in Figure 9c. At the region on the right bottom of Figure 9c, the proton transfer barrier is lowered due to the instability of C_s structure with large dihedral angle. The minima of structures with ring deformation found in Figures 7e and 8e, lies in this region. Thus, from the viewpoint of less frustration in the proton transfer reaction, structures with out-of-plane ring deformation are favorable as well as the planar structure. This indicates that the proton transfer drives the stability of the molecular structure of HM and DM. This is also confirmed by Figure 5b and e, which shows that the proton transfer seems to take place more frequently with structures with out-of-plane ring deformation than planar structures. Therefore, it may be suggested that the proton transfer plays a key role in the stabilization of the structures with out-of-plane ring deformation. We propose that the “proton transfer driven” mechanism is the origin of stabilization for the structure with out-of-plane ring deformation.

We roughly estimated the proton transfer barrier height for quantum simulation of HM and DM, and classical simulation at 300 K using statical calculation with fixed R_{OO} (and $R_{\text{OH}*}$ at the transition state).³³ The barrier height of DM lied in between that of HM and classical simulations. Thus, the proton transfer in the quantum simulation of DM can be affected by the barrier more than the case of HM and is less affected compared to classical simulation. The proton transfer barrier for quantum simulation of HM is completely washed out and is stable at planar configuration, while the barrier remains in classical simulation. We expect that proton transfer in quantum simulation of DM is not much affected by the barrier as classical simulation, and the proton transfer is washed out, as shown in Figure 4e. On the other hand, it is affected compared to quantum simulation of HM, so it favors the ring-distorted structure with less barrier height. This can be confirmed by Figure 5b and e, which shows that the proton transfer seems to take place more frequently with structures with out-of-plane ring deformation than planar structures. As a result, ring-distorted structure was found only for DM and not for HM.

4. CONCLUDING REMARKS

The present article features the nuclear quantum effect on the molecular structure and motion, especially the out-of-plane ring deformation of hydrogen maleate anion (HM) explored by *ab initio* PIMD simulations to study the existence of a stable structure with ring deformation, which was suggested in experimental observation.⁹ We investigated the degrees of freedom, which were not studied in previous studies.^{32–34} The isotope effect calculating the deuterated maleate anion (DM) is investigated as well. Temperature effect on the nuclear quantum effect is also examined by performing simulations at two different temperatures: 150 and 300 K.

The static calculation and classical *ab initio* molecular dynamics simulations have a dominant contribution from C_s symmetry hydrogen bond, or the hydrogen atom in the hydrogen bond is localized to either oxygen atom. In classical simulations, the proton transfer barrier remains in spite of the thermal fluctuation. On the other hand, trajectories in quantum *ab initio* PIMD simulation are dominated by C_{2v} symmetry hydrogen bond structure. Inclusion of the nuclear quantum effect result to a barrier-less proton transfer and the hydrogen bond atom is located at the center of two oxygen atoms.

Large isotope effect was found in the dihedral angle including the hydrogen bond in our *ab initio* PIMD simulations. Dihedral angle of DM was largely delocalized compared to HM, which indicates that out-of-plane ring distortion of DM is large. We also found in quantum simulation of DM that proton transfer takes place more frequently at distorted structures than in planar structures.

Principal component analysis was carried out to understand the nuclear quantum effect on molecular motion. The dominant motions were the out-of-plane ring bending modes, which correspond to the low-frequency modes found in normal-mode analysis. In quantum *ab initio* PIMD simulations, structures with ring deformation were the global minimum for DM at 300 K. Further analysis clarified that there are three minima along the out-of-plane ring bending mode with the largest contribution to the entire molecular motion for DM at 300 K. Our results, which found a stable structure with out-of-plane ring deformation, show agreement with the suggestion made by experimental observation employing inelastic neutron scattering.⁹ This is the first successful theoretical study to confirm the existence of a stable structure with out-of-plane ring deformation.

Finally, we investigated the origin of the stability for the structure with out-of-plane ring deformation. The structures with ring deformation corresponded to the structures with very small proton transfer barrier in static *ab initio* electronic structure calculation. We propose that the “proton transfer driven” mechanism is the origin of stabilization for the structure with out-of-plane ring deformation.

In this study, we have shown the capability of PIMD simulation for studying nuclear quantum effect on the entire molecule. However, we could not make direct comparison with experimental data in this study. There are many efforts made to study experimental IR spectra with molecular dynamics simulation.^{46,47,60} In our future works, we plan to study nuclear quantum effect on the molecular vibration using ring polymer molecular dynamics simulations,^{61,62} which enables us to construct IR spectra from time-correlation function.

■ AUTHOR INFORMATION

Corresponding Authors

*E-mail: yukio.kawashima@riken.jp.
*E-mail: tachi@yokohama-cu.ac.jp.

Present Address

[†](Y.K.) RIKEN Advanced Institute for Computational Science, 7-1-26, Minatojima-minami-machi, Chuo-ku, Kobe 650-0047, Japan

Notes

The authors declare no competing financial interest.

■ ACKNOWLEDGMENTS

The authors thank Professor F. Filliaux for kindly providing us the figure of their potential function (Figure 2). The authors also thank Dr. K. Yamada and Dr. K. Suzuki for helpful discussions. The present study has been supported by Grant-in-aid for Scientific Research by Ministry of Education, Culture, Sports, Science and Technology, Japan.

■ REFERENCES

- Peterson, S. W.; Levy, H. A. *J. Chem. Phys.* **1958**, *29*, 948–949.
- S. Darlow, S.; Cochran, W. *Acta Crystallogr.* **1961**, *14*, 1250–1257.

- (3) Cardwell, H. M. E.; Dunitz, J. D.; Orgel, L. E. *J. Chem. Soc.* **1953**, 3740–3742.
- (4) Nakamoto, K.; Sarma, Y. A.; Behnke, G. T. *J. Chem. Phys.* **1965**, 42, 1662–1667.
- (5) Zelmann, H. R.; Mielke, Z.; Ilczyszyn, M. M. *Spectrochim. Acta* **1988**, 44A, 705–708.
- (6) Ilczyszyn, M. M.; Baran, J.; Ratajczak, H.; Barnes, A. J. *J. Mol. Struct.* **1992**, 270, 499–515.
- (7) Tomkinson, J.; Braid, I. J.; Howard, J.; Waddington, T. C. *Chem. Phys.* **1982**, 64, 151–157.
- (8) Howard, J.; Tomkinson, J.; Eckert, J.; Goldstone, J. A.; Taylor, A. D. *J. Chem. Phys.* **1983**, 78, 3150–3155.
- (9) Fillaux, F.; Leygue, N.; Tomkinson, J.; Cousson, A.; Paulus, W. *Chem. Phys.* **1999**, 120, 387–403.
- (10) Forsen, S. *J. Chem. Phys.* **1959**, 31, 852–853.
- (11) Wong, A.; Pike, K. J.; Jenkins, R.; Clarkson, G. J.; Anupold, T.; Howes, A. P.; Crout, D. H. G.; Samoson, A.; Dupree, R.; Smith, M. E. *J. Phys. Chem. A* **2006**, 110, 1824–1835.
- (12) Fukai, M.; Matsuo, T.; Suga, H. *J. Chem. Thermodyn.* **1988**, 20, 1337–1347.
- (13) Olovsson, G.; Olovsson, I.; Lehmann, M. S. *Acta Crystallogr.* **1984**, C40, 1521–1526.
- (14) Perrin, C. L. *Pure Appl. Chem.* **2009**, 81, 571–583.
- (15) Perrin, C. L. *Science* **1994**, 266, 1665–1668.
- (16) Hall, G. E. *J. Am. Chem. Soc.* **1978**, 100, 8264–8266.
- (17) Schah-Mohammedi, P.; Shenderovich, I. G.; Deterring, C.; Limbach, H.-H.; Tolstoy, P. M.; Smirnov, S. N.; Denisov, G. S.; Golubev, N. S. *J. Am. Chem. Soc.* **2000**, 122, 12878–12879.
- (18) Latajka, Z.; Ratajczak, H. *Chem. Phys. Lett.* **1977**, 49, 407–419.
- (19) George, P.; Bock, C. W.; Trachtman, M. *J. Phys. Chem.* **1983**, 87, 1839.
- (20) Hodoscek, M.; Hadzi, D. *J. Mol. Struct. (Theochem)* **1990**, 209, 411.
- (21) Rios, M. A.; Rodriguez, J. *Can. J. Chem.* **1993**, 71, 303–306.
- (22) Garcia-Viloca, M.; Gonzalez-Lafont, A.; Lluch, J. M. *J. Am. Chem. Soc.* **1997**, 119, 1081–1086.
- (23) Garcia-Viloca, M.; Gonzalez-Lafont, A.; Lluch, J. M. *J. Am. Chem. Soc.* **1999**, 121, 9198–9207.
- (24) Bach, R. D.; Dmitrenko, O.; Glukhovtsev, M. N. *J. Am. Chem. Soc.* **2001**, 123, 7134–7145.
- (25) Woo, H.-K.; Wang, X.-B.; Wang, L.-S.; Lau, K.-C. *J. Phys. Chem. A* **2005**, 109, 10633–10637.
- (26) Tian, S. X.; Li, H.-B. *J. Phys. Chem. A* **2007**, 111, 4404–4410.
- (27) Avbelj, F.; Hodoscek, M.; Hadzi, D. *Spectrochim. Acta* **1985**, 41A, 89–97.
- (28) Ratajczak, H.; Barnes, A.; Baran, J.; Yaremko, A.; Latajka, Z.; Dopieralski, P. *J. Mol. Struct. (Theochem)* **2008**, 887, 9–19.
- (29) Vener, M. V.; Manaev, A. V.; Tsirelson, V. G. *J. Phys. Chem. A* **2008**, 112, 13628–13632.
- (30) Wilson, C. C.; Thomas, L. H.; Morrison, C. A. *Chem. Phys. Lett.* **2003**, 381, 102–108.
- (31) Wilson, C. C.; Thomas, L. H.; Morrison, C. A. *Chem. Phys. Lett.* **2004**, 399, 292–293.
- (32) Dopieralski, P.; Perrin, C. L.; Latajka, Z. *J. Chem. Theory Comput.* **2011**, 7, 3505–3513.
- (33) Kawashima, Y.; Tachikawa, M. *Chem. Phys. Lett.* **2013**, 571, 23–27.
- (34) Gerlt, J. A.; Gassman, P. G. *Biochemistry* **1993**, 32, 11943–11952.
- (35) Cleland, W. W.; Kreevoy, M. M. *Science* **1994**, 264, 1887–1890.
- (36) Frey, P. A.; Whitt, S. A.; Tobin, J. B. *Science* **1994**, 264, 1927–1930.
- (37) Shan, S. O.; Loh, S.; Herschlag, D. *Science* **1996**, 272, 97–101.
- (38) Yamaguchi, S.; Kamikubo, H.; Kurihara, K.; Kuroki, R.; Niimura, N.; Yamazaki, Y.; Kataoka, M. *Proc. Natl. Acad. Sci. U.S.A.* **1996**, 106, 440–444.
- (39) Scheiner, S.; Kar, T. *J. Am. Chem. Soc.* **1995**, 117, 6970–6975.
- (40) Marx, D.; Parrinello, M. *Z. Phys. B: Condens. Matter* **1994**, 95, 143–144.
- (41) Marx, D.; Parrinello, M. *J. Chem. Phys.* **1996**, 104, 4077–4082.
- (42) Shiga, M.; Tachikawa, M.; Miura, S. *Chem. Phys. Lett.* **2000**, 332, 396–402.
- (43) Shiga, M.; Tachikawa, M.; Miura, S. *J. Chem. Phys.* **2001**, 115, 9149–9159.
- (44) Tachikawa, M.; Shiga, M. *J. Am. Chem. Soc.* **2005**, 127, 11908–11909.
- (45) Suzuki, K.; Shiga, M.; Tachikawa, M. *J. Chem. Phys.* **2008**, 129, 144310.
- (46) Møller, K. B.; Rey, R.; Hynes, J. T. *J. Phys. Chem. A* **2004**, 108, 1275–1289.
- (47) Rey, R.; Møller, K. B.; Hynes, J. T. *J. Phys. Chem. A* **2002**, 106, 11993–11996.
- (48) Kamerlin, S. C. L.; Mavri, J.; Warshel, A. *FEBS Lett.* **2010**, 584, 2759–2766.
- (49) Chai, J.-D.; Head-Gordon, M. *Phys. Chem. Chem. Phys.* **2008**, 10, 6615–6620.
- (50) Martyna, G. J.; Klein, M. L.; Tuckerman, M. E. *J. Chem. Phys.* **1992**, 97, 2635–2643.
- (51) Tuckerman, M. E.; Marx, D.; Klein, M. L.; Parrinello, M. *J. Chem. Phys.* **1996**, 104, 5579–5588.
- (52) Frisch, M. J.; Trucks, G. W.; Schlegel, H. B.; Scuseria, G. E.; Robb, M. A.; Cheeseman, J. R.; Scalmani, G.; Barone, V.; Mennucci, B.; Petersson, G. A.; Nakatsuji, H.; Caricato, M.; Li, X.; Hratchian, H. P.; Izmaylov, A. F.; Bloino, J.; Zheng, G.; Sonnenberg, J. L.; Hada, M.; Ehara, M.; Toyota, K.; Fukuda, R.; Hasegawa, J.; Ishida, M.; Nakajima, T.; Honda, Y.; Kitao, O.; Nakai, H.; Vreven, T.; Montgomery, J. A., Jr.; Peralta, J. E.; Ogliaro, F.; Bearpark, M.; Heyd, J. J.; Brothers, E.; Kudin, K. N.; Staroverov, V. N.; Kobayashi, R.; Normand, J.; Raghavachari, K.; Rendell, A.; Burant, J. C.; Iyengar, S. S.; Tomasi, J.; Cossi, M.; Rega, N.; Millam, J. M.; Klene, M.; Knox, J. E.; Cross, J. B.; Bakken, V.; Adamo, C.; Jaramillo, J.; Gomperts, R.; Stratmann, R. E.; Yazyev, O.; Austin, A. J.; Cammi, R.; Pomelli, C.; Ochterski, J. W.; Martin, R. L.; Morokuma, K.; Zakrzewski, V. G.; Voth, G. A.; Salvador, P.; Dannenberg, J. J.; Dapprich, S.; Daniels, A. D.; Farkas, ; Foresman, J. B.; Ortiz, J. V.; Cioslowski, J.; Fox, D. J. *Gaussian 09*, Revision B.02; Gaussian Inc.: Wallingford, CT, 2009.
- (53) Kitao, A.; Hirata, F.; Go, N. *Chem. Phys.* **1991**, 158, 447–472.
- (54) Garcia, A. E. *Phys. Rev. Lett.* **1992**, 68, 2696–2699.
- (55) Amadei, A.; Linssen, A. B. M.; Berendsen, H. J. C. *Proteins* **1993**, 17, 412–425.
- (56) Kitao, A.; Go, N. *Curr. Opin. Struct. Biol.* **1999**, 9, 164–169.
- (57) Flyvbjerg, H.; Petersen, H. G. *J. Chem. Phys.* **1989**, 91, 461–466.
- (58) Tuckerman, M. E.; Marx, D. *Phys. Rev. Lett.* **2001**, 86, 4946–4949.
- (59) Pirc, G.; Stare, J.; Mavri, J. *J. Chem. Phys.* **2010**, 132, 224506.
- (60) Pirc, G.; Mavri, J.; Novič, M.; Stare, J. *J. Phys. Chem. B* **2012**, 116, 7221–7231.
- (61) Craig, I. R.; Manolopoulos, D. E. *J. Chem. Phys.* **2004**, 121, 3368.
- (62) Shiga, M.; Nakayama, A. *Chem. Phys. Lett.* **2008**, 451, 175–181.